Check for updates

A novel fluorescent probe, triphenylamine rhodamine-3-acetic acid (mRA) for the detection of Amyloid-β aggregates in Alzheimer's disease

Raja Chinnappan[1,2]*, Mateen A. Khan[3]*, Taj Mohammad[4], Sarah Mohammed Allwaibh[3], Shanmugam Easwaramoorthi[5], Ahmed Yaqinuddin[1], Sandhanasamy Devansan[6], Tanveer Ahmad Mir[1,2] and Imtaiyaz Hassan[4]

[1]College of Medicine, Alfaisal University, Riyadh, Saudi Arabia, [2]Tissue/Organ Bioengineering & BioMEMS Laboratory, Organ Transplant Centre of Excellence (TR & I-Dept), King Faisal Specialist Hospital and Research Centre, Riyadh, Saudi Arabia, [3]Department of Life Sciences, College of Science and General Studies, Alfaisal University, Riyadh, Saudi Arabia, [4]Center for Interdisciplinary Research in Basic Sciences, Jamia Millia Islamia, Jamia Nagar, New Delhi, India, [5]Inorganic and Physical Chemistry Lab, CSIR-Central Leather Research Institute, Adyar, Chennai, India, [6]Bioproducts Research Chair, Department of Zoology, College of Science, King Saud University, Riyadh, Saudi Arabia

Amyloid-β (Aβ) is implicated in the pathophysiology of Alzheimer's disease (AD) and plays a significant role in neuronal degeneration. Aβ in solution is essential during the initial stages of developing lead compounds that influence Aβ fibrillation. The tendency of the Aβ peptide to misfold in solution is correlated with the etiology of AD. Therefore, the early detection of Aβ serves as a critical foundation for diagnostic testing and routine clinical assessment of AD. Herein, an aggregation-induced fluorescence probe, triphenylamine rhodamine-3-acetic acid (mRA), was used to detect Aβ aggregates. The fluorescence results showed a strong interaction between the fluorescence probe mRA and Aβ aggregates. mRA specifically binds with high affinity to Aβ aggregates, and the limit of detection (LOD) of Aβ aggregates was $0.12\,\mu g/mL$. Molecular docking studies showed that the mRA has significant binding affinity toward the Aβ peptide at the N/C-terminal region, with a binding energy of -6.5 kcal/mol. Furthermore, CD studies confirmed that the mRA binds to Aβ aggregates, and its binding induces significant structural alteration of the Aβ aggregates. Thermodynamic properties revealed that the binding of Aβ aggregates to mRA is a spontaneous process, driven by enthalpy and favored by entropy, which helps further our understanding of the interaction between mRA and Aβ aggregates at the molecular level. The negative ΔH suggests that hydrogen bonding is a dominant force for the mRA interaction with Aβ aggregates. This study provides a rationale for using mRA as a biosensor for the detection of Aβ aggregates in biological fluids, offering a potential tool for the early diagnosis and monitoring of amyloid progression in AD.

KEYWORDS

Alzheimer's disease, mRA, fluorescent sensing probe, binding, thermodynamics, molecular docking, conformational change

1 Introduction

Alzheimer's disease (AD) is a neurodegenerative condition marked by amyloid plaques and neurofibrillary tangles building up and progressive neuronal destruction (Scheltens et al., 2016; Hampel et al., 2021). In contrast to internal neurofibrillary tangles, which are composed of aggregated phosphorylated tau, external amyloid plaques have been found to consist mostly of aggregated Amyloid-β (Aβ) (Avila et al., 2004). The main component of senile plaques in AD brains is the longest and most hydrophobic. In a normal human brain, $A\beta_{1-40}$ is predominant; however, in disease conditions, excess $A\beta_{1-42}$ is found in cerebrospinal fluid (CSF) and predominantly accumulated as amyloid plaques. A soluble Aβ is derived from amyloid precursor protein (APP) (integral membrane protein) by the amyloidogenic pathway's successive cleavage of β-secretase and γ-secretase (Selkoe, 2001). However, depending on the physiological environment, Aβ can accumulate into soluble oligomers and protofibrillar intermediates, which subsequently aggregate into insoluble fibrils and amyloid plaques. The $A\beta_{1-42}$ has severe neurotoxicity and possesses faster aggregation kinetics compared to $A\beta_{1-40}$ (Kayed et al., 2009). The reduction of soluble Aβ due to its oligomerization and aggregation may serve as an early biomarker for Alzheimer's disease (AD). Abnormal synthesis and accumulation of Aβ in blood plasma and cerebrospinal fluid (CSF) are key pathological events contributing to the progression of AD. The deposition of amyloid on neurons leads to neurodegeneration and cognitive decline, which are hallmarks of dementia and early indicators of Alzheimer's disease. Therefore, routine clinical analysis and personalized treatment strategies rely on the early and accurate detection of amyloid species in CSF and other biological fluids (Scheme 1). Among the various Amyloid-Beta isoforms, $A\beta_{1-42}$ is the principal component involved in amyloid plaque formation and represents a promising biomarker for monitoring Alzheimer's disease progression. The detection of Aβ levels in human cerebrospinal fluid (CSF) has been widely validated as a reliable biomarker for the diagnosis of Alzheimer's disease, including at its earliest clinical stages (Qin et al., 2018).

Traditional imageology tests and clinical symptoms are the primary methods used to diagnose AD. However, because of its gradual onset, symptoms frequently develop later than the disease progresses (Nasica-Labouze et al., 2015). For the early diagnosis and treatment of AD, it is crucial to create non-invasive, quick, and trustworthy methods. Various techniques and attempts have been made for screening Aβ. The enzyme-linked immunosorbent assay (ELISA) is widely used to measure Aβ peptides (Barghorn et al., 2005). Recently, an electrochemical and fluorescence sensing methodology has been widely adopted for probing Aβ aggregation and its interaction with biomolecules (Qin et al., 2018; Sharma et al., 2022). Several nanomaterials were created to find biomarkers based on CSF (Qin et al., 2019). Raman dye-coated polyA aptamer-AuNPs and the surface-enhanced Raman scattering (SERS) technology have been used to produce a SERS biosensor platform for the detection of $A\beta_{1-42}$. These techniques are cumbersome for point-of-care applications with limited resources. The fluorescence technique has numerous advantages over these other technologies, including quantitative detection, low-cost equipment, real-time analysis, remote detection capability, specificity, high sensitivity, and no sample preparation complexity. Moreover, fluorescent methods provide longer-term, real-time biointeraction monitoring and are non-invasive (Kubota and Hamachi, 2015).

Biosensors have been crucial in identifying Aβ aggregates and monomers in recent years. Aβ in CSF and blood samples has been measured using the current detection techniques, which are based on electrochemical, surface plasmon resonance (SPR), SERS, and colorimetric sensors. As a novel approach for the quantitative measurement of Aβ, fluorescent probe sensors have garnered increasing attention due to their high sensitivity, rapid response times, and suitability for Aβ detection and analysis (Ren et al., 2020; Fang et al., 2023). Moreover, fluorescent dyes are relatively easy to design, modify, and synthesize. A variety of turn-on and environment-sensitive probes have been developed. Several fluorescent probes have demonstrated enhanced selectivity and photostability, offering improved performance for detecting Aβ aggregates in complex biological environments (Zhang et al., 2021; Mallesh et al., 2022, 2023). Aggregation-induced emission (AIE) probes display minimal background signal and selectively light up upon binding to Aβ aggregates (Fang et al., 2023). Furthermore, Förster resonance energy transfer (FRET)-based biosensors have enabled real-time monitoring of Aβ aggregation (Trusova et al., 2022). These advances highlight the growing utility of fluorescence probe–based methods in both fundamental research and potential diagnostic applications for AD.

Recently, fluorescence turn-on probes have been employed for the detection of Aβ, with Thioflavin T (ThT) and Congo Red being among the most commonly used for quantitative detection of $A\beta_{1-4_2}$ (Howie and Brewer, 2009). ThT, in particular, is often considered the gold standard to detect aggregated $A\beta_{1-40}$ and $A\beta_{1-4_2}$ and other fibrillary aggregates. However, its low binding affinity, limited selectivity, and poor specificity have driven the development of more effective fluorescent probes. In response to these limitations, a novel fluorescent molecule, Triphenylamine Rhodamine-3-Acetic Acid (mRA), has been designed and synthesized for the selective detection of Aβ aggregates.

In this study, we developed a turn-on fluorescence probe, mRA, for the selective detection of trace levels of $A\beta_{1-42}$ aggregates in bodily fluids based on changes in the fluorescence-sensitive local microenvironment within the $A\beta_{1-42}$ aggregates mRA complex fluorescence. mRA has weak fluorescence in PBS buffer; however, a strong emission signal is observed upon binding to Aβ aggregates. The well-designed fluorescent probe mRA selectively and sensitively recognizes $A\beta_{1-42}$, exhibiting high binding affinity and excellent thermostability in the resulting complex. This study provides a relevant sensing approach for the growing number of dyes binding small molecules to assist in the early detection of Aβ aggregates in AD.

2 Materials and methods

2.1 Materials

Triphenylamine rhodamine-3-acetic (mRA) dye was synthesized as described previously (Thamaraiselvi et al., 2019). The Aβ protein was purchased from OriGene (Rockville, MD, USA). The concentration of protein was determined following the
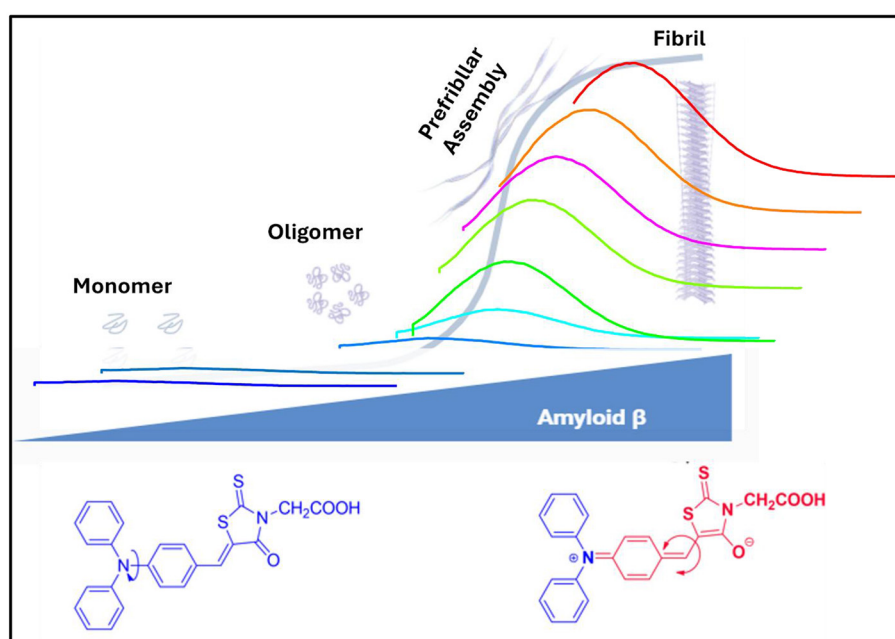
SCHEME 1
Schematic representation of monitoring the Aβ protein by fluorescence probe mRA.

standard Bradford method (Bradford, 1976). All buffers were made up in Milli-Q water with a resistivity of 18.2 MΩ.cm. All the other chemicals used in this study were of molecular biological grade.

2.2 Steady state fluorescence measurement

Fluorescence spectroscopy was used to determine the strength of binding affinity of the fluorescence probe, mRA, with Aβ protein. The fluorescence probe mRA bound to Aβ was observed in the emission range of 510–750 nm by exciting the complex at 475 nm. The excitation and emission slits were set at 5 and 10 nm, respectively, with a cuvette path length of 1 cm. In the fluorescence experiments, Aβ concentrations were varied from 0 to 300 μg/mL, while the constant concentration of mRA was maintained at 2.5 μM. All spectral measurements were made after incubating mRA-Aβ$_{1-42}$ in PBS buffer (pH 7.4) for 15 min to keep the necessary temperature constant. A linear relationship was observed between Aβ$_{1-42}$ and mRA, as demonstrated by a linear plot of Aβ$_{1-42}$ concentration vs. mRA fluorescence intensity. The minimum detectable amount of Aβ$_{1-42}$, or the limit of detection (LOD), was calculated using the standard formula:

$$LOD = \frac{3.3\sigma}{S}$$

Where σ is the standard deviation of the blank signal (without BSA); S is the slope of the calibration plot.

All sample binding investigations were conducted at 25°C under dim light to protect from photo-oxidation of the fluorescent probe. A thermocouple device was used to control the cuvette holding sample temperature ($\Delta T \pm 0.1°C$). The titration of

mRA with increasing Aβ concentrations was carried out in a discontinuous manner. To a fixed concentration of mRA (2.5 μM), increasing amounts of Aβ were added from 0 to 300 μg/mL. After adding Aβ, the changes in mRA fluorescence intensity data were analyzed by fitting them using the following equation:

$$\Delta F = (F_0 - F_f)/F_0 \qquad (1)$$

Where ΔF is the change in fluorescence enhancement seen in any sample; the fluorescence intensity of mRA alone (control) is denoted by F_0; F_f denotes the fluorescence enhancement after adding Aβ. To account for the background signal, the fluorescence of Aβ$_{1-42}$ alone in PBS buffer was subtracted from the measured fluorescence intensities of the Aβ$_{1-42}$/mRA complex. The resulting corrected fluorescence values were then used to calculate the binding affinity of the complex. The equilibrium binding affinity ($K_a = 1/K_d$) was determined using the normalized fluorescence values ($\Delta F/\Delta F_{max}$), where ΔF_{max} represents the maximum fluorescence change corresponding to complete saturation of mRA by Aβ$_{1-42}$. To determine ΔF_{max}, a $1/\Delta F$ vs. $1/[A\beta]$ plot was extrapolated to the ordinate for the intercept (Khan et al., 2023). The equilibrium measurement was conducted using three independent titration trials. K_d values were acquired by KaleidaGraph using non-linear regression analysis.

We further investigated the temperature-dependent Aβ binding to mRA. This assay was carried out at four distinct temperatures (288, 293, 298, and 310 K) under the same standard experimental conditions as the fluorescence titration described above. The experimental temperature was maintained for each sample using a temperature controller.

2.3 Thermodynamic measurements

To better understand the mechanism of interaction for the binding forces involved in the binding of mRA and $A\beta_{1-42}$ aggregates, thermodynamic measurements were performed. Temperature-dependent binding constant for the mRA-$A\beta_{1-42}$ aggregates complex formation was monitored by the fluorescence measurements as described previously (Khan et al., 2017). Change in enthalpy (ΔH) and entropy (ΔS) between $A\beta_{1-42}$ aggregates-mRA were determined by Van't Hoff equation. Equation (3) was used to calculate the change in Gibbs free energy involved in an $A\beta_{1-42}$/mRA complex formation.

$$ln\, K_a \,=\, -\frac{\Delta H}{R\,T} + \frac{\Delta S}{R} \qquad (2)$$

$$\Delta G = -\,R\,T\,ln\,K_a = \Delta H - T\Delta S \qquad (3)$$

Where K_a is the binding constant; ΔH and ΔS are the enthalpy and entropy change; ΔG is the Gibbs free energy; T is the absolute temperature; R is the universal gas constant (1.987 Cal mol^{-1} K^{-1}). The intercept and slope of a plot of ln K_a vs. the inverse of temperature yielded $-\Delta H/R$ and $\Delta S/R$.

2.4 Circular dichroism spectroscopy

Far-UV circular dichroism (CD) spectra of native $A\beta$ protein and $A\beta_{1-42}$/mRA were observed with a spectropolarimeter. We employed a thermo-controller with a circulating water bath to keep the temperature at 298 K under a continuous flow of nitrogen gas with a slit width of 2 nm. As directed by the manufacturer, D-10-camphorsulphonic acid was used to calibrate the instrument. Changes in ellipticity were obtained at a fixed $A\beta_{1-42}$ concentration (1 μM) and in the presence of varying amounts of mRA (0–10 μM). After 15 min of incubation, spectra were recorded for each sample.

Each CD spectrum was acquired using a 0.1 cm quartz cell in the wavelength range of 190–260 nm. The instrument response time was one second with a recording rate of 100 nm/min. Each spectrum was obtained by averaging five scans before the final spectral collection. Each collected spectrum was corrected by subtracting the corresponding contributions from the buffer alone and, when applicable, the $A\beta_{1-42}$/mRA complex in buffer. The obtained spectra were confirmed by eliminating a buffer background scan from the initial protein spectrum. Every spectrum having a bandwidth of 60 was subjected to the SG filter. Each spectrum data set was displayed as mean residual ellipticity vs. wavelength (nm) as a function of (deg.cm^2.dmol^{-1}). The change in the intensity of the free $A\beta_{1-42}$ ellipticity upon addition of mRA suggests a conformational change in the $A\beta_{1-42}$ sample in the presence of different mRA concentrations, which was calculated using the CDNN tool.

2.5 Molecular docking analysis

Molecular docking studies were conducted to investigate the binding of mRA with $A\beta_{42}$ residue peptide (APPβ) using Insta Dock v1.2 (Mohammad et al., 2021). The solution structure of the $A\beta$ peptide (1-42) was retrieved from the RCSB Protein Data Bank (PDB ID: 1Z0Q) (Bank, 1971). The structures were prepared by adding hydrogen atoms, assigning charges, and defining appropriate atom types. A blind docking approach, covering the entire APPβ proteins, was adopted to identify binding sites. The 2D molecular structure of mRA was drawn using ChemBioDraw Ultra 14.0 and converted to a 3D structure, followed by geometry optimization using the MMFF94 force field before docking (Supplementary Figure S1). Flexible docking simulations employed grid dimensions of 58 Å × 51 Å × 30 Å for $A\beta$ peptide, centered at coordinates (−5.364, −0.161, −5.029). The grid spacing was set to 1.00 Å, and the exhaustiveness parameter was adjusted to 8 for thorough conformational sampling. Docking simulations were executed with default parameters, ranking the resulting poses based on binding affinity and interaction energy. Key interactions between mRA and amino acid residues in the binding sites were analyzed. The top-ranked conformations were processed using the InstaDock Splitter program, and detailed binding modes were visualized using PyMOL (DeLano, 2002) and Discovery Studio Visualizer (Visualizer, 2005).

3 Results and discussion

3.1 Interaction of mRA probe with Aβ protein

Binding interactions between the mRA probe and $A\beta$ were examined through fluorescence enhancement titration, molecular docking studies, CD spectroscopy, and specificity and cross-reactivity analyses. It is known that $A\beta_{1-42}$ exhibits different forms of aggregation in increasing concentrations, and the aggregated forms interact with the probe and influence their fluorescence behavior (Scheme 1). Excitation of mRA/$A\beta_{1-42}$ aggregate complex at 475 nm produced a fluorescence in the range of 500–750 nm with an emission peak at 575 nm. Figure 1A shows fluorescence emission spectra of mRA in the presence of increasing concentrations of $A\beta_{1-42}$. A fixed concentration of mRA (2.5 μM) was titrated with varying amounts of $A\beta_{1-42}$ in the range of 0–300 μg/mL. A concentration-dependent increase in fluorescence intensity was observed with $A\beta$, suggesting an interaction with mRA that alters its fluorescence characteristics. As reported previously, the critical aggregation concentration (CAC) of $A\beta_{1-42}$ is 90 nM (Novo et al., 2018). The observed enhancement in fluorescence intensity suggests that monomeric $A\beta_{1-42}$ undergoes progressive aggregation into various forms, such as oligomers, prefibrillar assemblies, protofilaments, and mature fibrils as its concentration increases. The maximum fluorescence intensity observed at 300 μg/mL of $A\beta_{1-42}$ indicates that the mRA probe exhibits a stronger interaction with mature fibrils compared to other aggregate forms. Figure 1B depicts a linear relationship established between the concentration of $A\beta_{1-42}$ and the fluorescence response of mRA. The limit of detection (LOD), calculated from the linear plot, was determined to be 0.12 μg/mL.

By directly titrating $A\beta$ with limiting mRA concentration, the interaction between $A\beta$ and mRA was observed in equilibrium conditions. Figure 2 shows the binding of mRA with the
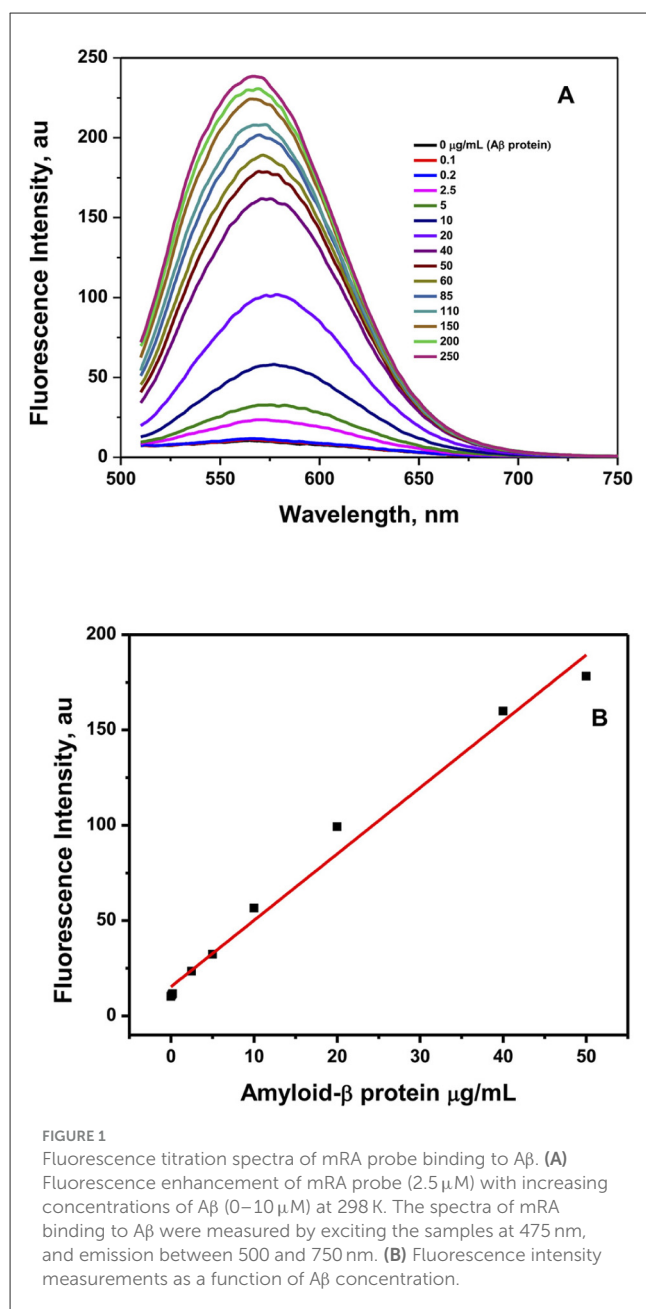
FIGURE 1
Fluorescence titration spectra of mRA probe binding to Aβ. **(A)** Fluorescence enhancement of mRA probe (2.5 μM) with increasing concentrations of Aβ (0−10 μM) at 298 K. The spectra of mRA binding to Aβ were measured by exciting the samples at 475 nm, and emission between 500 and 750 nm. **(B)** Fluorescence intensity measurements as a function of Aβ concentration.

increasing amounts of Aβ$_{1-42}$. The addition of Aβ$_{1-42}$ protein significantly enhanced the fluorescence intensity of the mRA probe. Fluorescence change revealed the protein and ligand binding, which promotes a change in orientation of the protein molecule induced by Aβ$_{1-42}$ binding. Fluorescence enhancement of the mRA was observed when Aβ concentration increased. The peak for the native mRA sensor was located at 575 nm. On the other hand, mRA fluorescence increased as the quantity of Aβ$_{1-42}$ increased, indicating the formation of an mRA/Aβ$_{1-42}$ aggregate complex. The mRA sensor binds to Aβ$_{1-42}$ with a significant binding affinity. The binding affinity for the mRA interaction to Aβ$_{1-42}$ was 3.0×10^6 M^{-1} at 298 K. The fluorescence data were analyzed by fitting them into binding plots as described in the method section.

In the early stages, Congo red, a deep crimson dye, was used for the detection of Aβ$_{1-42}$. However, due to their poor performance and practical challenges, these dyes are being replaced by other efficient probes. Vassar and Culling demonstrated the diagnosis of amyloid fibrils by an amyloid-specific fluorescence probe called Thioflavin-T (ThT) by fluorescent microscopy (Puchtler et al., 1959). A drastic enhancement in the fluorescence upon binding to amyloid fibrils is explained by the selective immobilization of a specific group of the ThT molecule, and it behaves as a "molecular rotor." Similar characteristic behavior of mRA was observed in the previous studies (Thamaraiselvi et al., 2019; Chinnappan et al., 2025). In the solution, the single bond between the nitrogen and the phenyl group attached to the acceptor moiety was rotating freely and rapidly, which leads to quenching the excited state and reducing the fluorescence emission. In contrast, the excited state mRA in the mRA/Aβ$_{1-42}$ aggregate complex is unaffected by the quencher; the free rotational immobilization of the quencher in the complex does not influence the excited state of mRA, resulting in high fluorescence emission. As the concentration of Aβ increases, it forms strong amyloid fibrils that sterically lock the mRA probe (Figure 1). Therefore, the fluorescence emission increases proportionally to Aβ concentration.

Furthermore, using an intrinsic fluorescence assay at different temperatures (288, 293, 298, and 310 K), the binding characteristics of the mRA/Aβ$_{1-42}$ aggregate interaction were investigated. The temperature-dependent binding affinity was used to evaluate the details of the mRA/Aβ$_{1-42}$ aggregate's effective mechanism of interaction. Addition of Aβ$_{1-42}$ to mRA at variable temperatures showed significant enhancement of mRA fluorescence, revealing that mRA binds to Aβ$_{1-42}$ at different temperatures. Temperature-dependent binding parameters can offer insight into the operative mode of mRA/Aβ$_{1-42}$ aggregate interaction. Figure 3 shows a summary of the binding affinity plot for mRA/Aβ binding at varying temperatures (Table 1). An increase in temperature led to a corresponding increase in the dissociation constant K_{d}, indicating that mRA and Aβ form a dynamic, reversible complex. Specifically, the K_{d} increased from 178 ± 8.7 nM at 288 K to 515 ± 18 nM at 310 K, suggesting that the mRA/Aβ$_{1-42}$ aggregate complex is more stable at lower temperatures. This temperature-dependent behavior highlights the thermally labile nature of the interaction. The K_d value of the mRA/Aβ$_{1-42}$ aggregate binding at 310 K was greater than that at 288 K, according to fluorescence data analysis (Table 1). It was evident that the K_d increased with temperature, indicating a dynamic mode of interaction between mRA and Aβ$_{1-42}$ aggregates.

3.2 Thermodynamics of mRA probe and Aβ binding

Thermodynamic features o the complex formation were investigated to gain a better understanding of the mechanism underlying an mRA/Aβ$_{1-42}$ interaction. The stability of the mRA/Aβ$_{1-42}$ β combination was evaluated utilizing thermodynamic parameters. By calculating binding affinity at various temperatures, the thermodynamics of the mRA/Aβ$_{1-42}$ interaction aids in our understanding of the types of forces that lead to complex formation. Figure 4A shows Van't Hoff graph
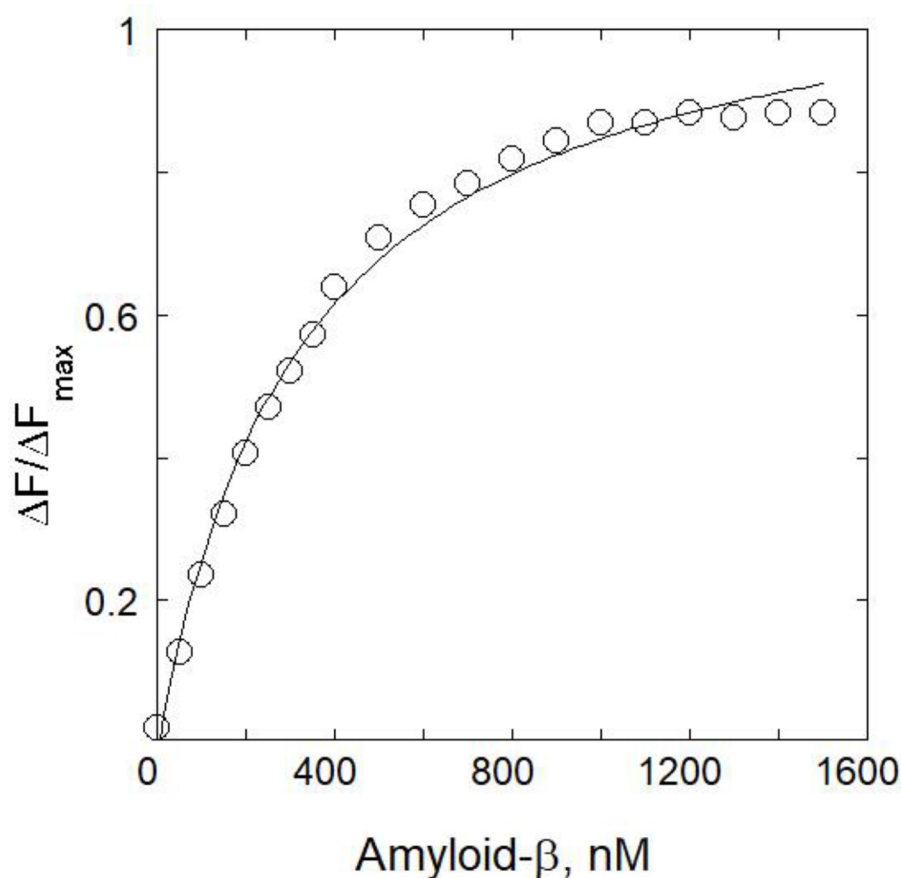
FIGURE 2
The mRA probe strongly interacts with the Aβ-peptide. Direct fluorescence titration of Aβ at 25°C was used to measure the affinity of mRA for Aβ. Various amounts of Aβ were incubated with constant mRA (1 μM) to prepare the samples.

with T_{-1} on the x-axis and lnKa on the y-axis for the binding of mRA with $A\beta_{1-42}$. Using the calculated K_a values in Table 1, the experimental temperature T, and the gas constant R, linear analysis of the Van't Hoff graph yielded results for enthalpy and entropy change. The slope provides the value of enthalpy change, and the intercept gives the value of $\triangle S$. A small positive entropy ($\triangle S = 0.8 \pm 0.04$ cal mol^{-1} K^{-1}) and a substantial negative enthalpy ($\triangle H = 8.7 \pm 0.5$ kcal mol-1) indicated that the interactions are enthalpically driven and favored by entropy (Khan et al., 2017). Additionally, $\triangle H$ negative (<0) and $T\triangle S$ positive (>0) revealed that hydrogen bonding and van der Waals forces are the dominant forces involved in stabilizing mRA/$A\beta_{1-42}$ aggregate complex formation.

The ΔG is a thermodynamic indicator of a binding reaction's spontaneity. A negative ΔG value indicates that the mRA/$A\beta_{1-42}$ aggregate complex forms spontaneously under normal conditions. Figure 4 shows the thermodynamic characteristics of mRA binding to Aβ. The value of ΔG at 25°C was estimated using the variables from Table 2 and Equation 2. For the mRA/$A\beta_{1-42}$ aggregate complex, the calculated value of ΔG was -9.3 ± 0.6 kcal mol^{-1}. Additionally, molecular docking offers a thorough examination of the residues and forces that are essential to mRA/$A\beta_{1-42}$ aggregate interactions.

The negative ΔG value thermodynamically favors the mRA interaction with $A\beta_{1-42}$. Both entropically (7.5%) and enthalpically (93%), the interaction between mRA and $A\beta_{1-42}$ is advantageous, with an 85% higher enthalpic contribution to ΔG at 25°C. The involvement of the protein-ligand bonding forces was dependent on the sign and magnitude of the thermodynamic parameters (Ross and Subramanian, 1981; Khan, 2022). Additionally, a significant negative ΔH suggests that hydrogen bonding and van der Waals contact are the main driving forces that cause the formation of the mRA/$A\beta_{1-42}$ aggregate complex (Ross and Subramanian, 1981; Tayyab et al., 2019). However, mRA/$A\beta_{1-42}$ aggregate complexes showed a low $T\Delta S$ value, revealing the absence of hydrophobic forces.

3.3 mRA probe-induced conformational changes in Aβ protein

At the secondary structural level of the protein, CD offers vital information on protein conformational properties. Using CD spectroscopy, one can examine structural alterations in proteins
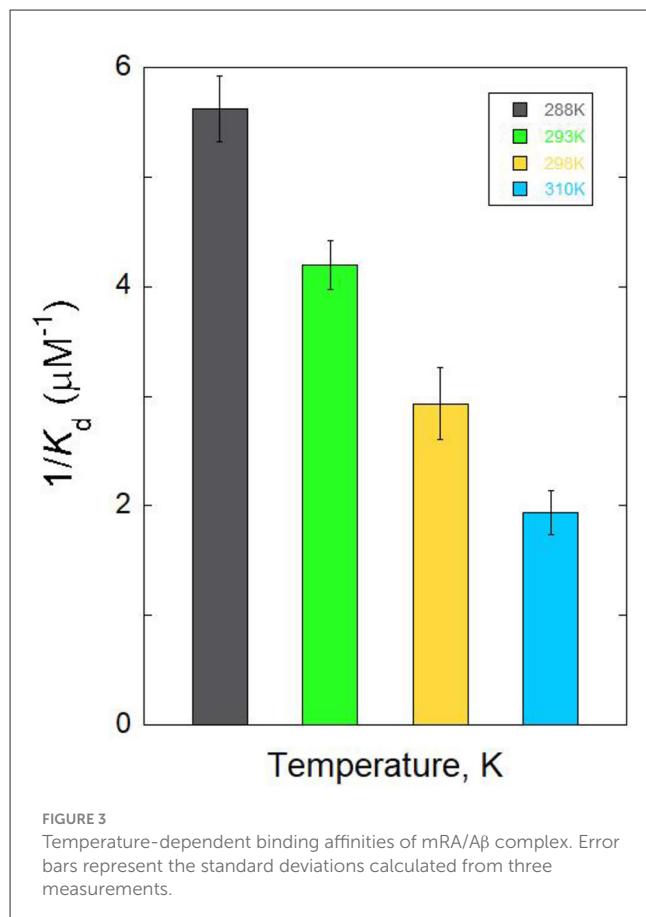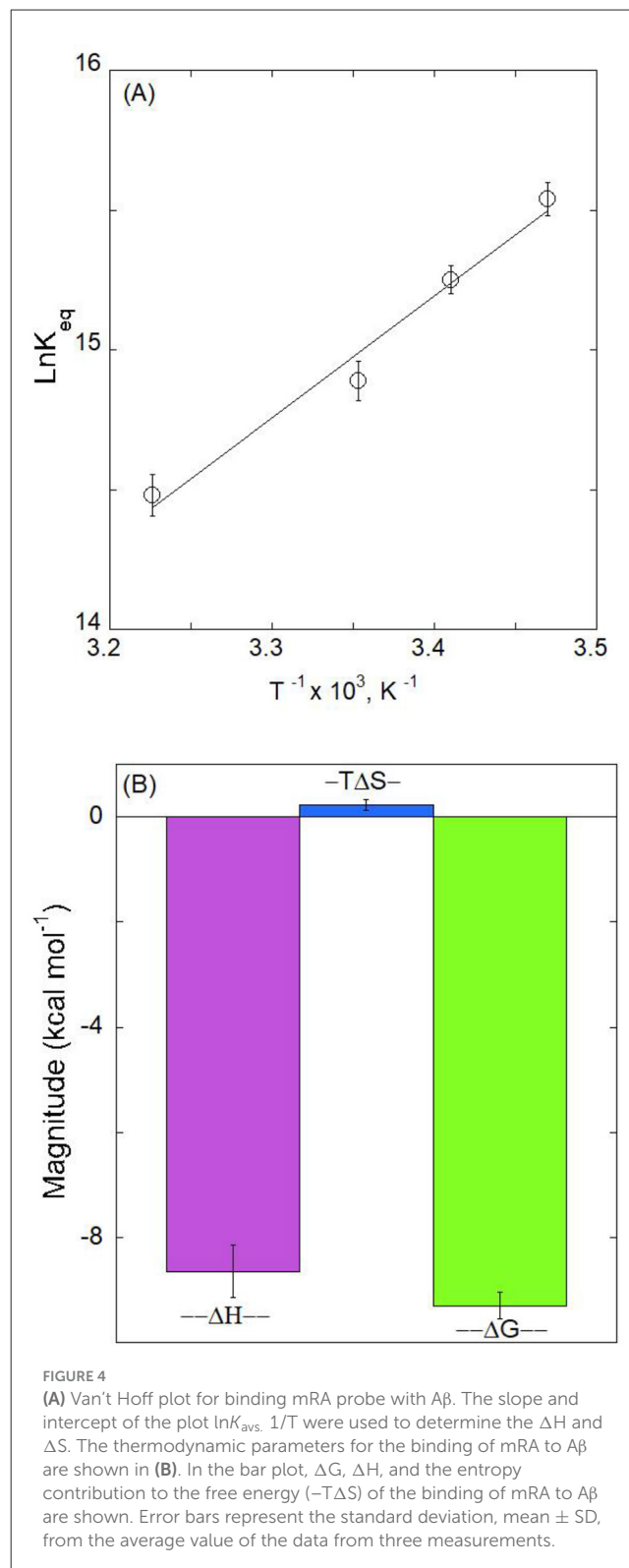
FIGURE 3
Temperature-dependent binding affinities of mRA/Aβ complex. Error bars represent the standard deviations calculated from three measurements.

TABLE 1 Dissociation constants (K_d) for the binding of mRA probe with Aβ protein.

Complex	K_d (nM)			
	288 K	293 K	298 K	310 K
Aβ-mRA	178 ± 8.7	239.7 ± 11	341 ± 17	515 ± 18

FIGURE 4
(A) Van't Hoff plot for binding mRA probe with Aβ. The slope and intercept of the plot $\ln K_{avs.}$ 1/T were used to determine the ΔH and ΔS. The thermodynamic parameters for the binding of mRA to Aβ are shown in (B). In the bar plot, ΔG, ΔH, and the entropy contribution to the free energy (−TΔS) of the binding of mRA to Aβ are shown. Error bars represent the standard deviation, mean ± SD, from the average value of the data from three measurements.

that result from interactions with ligands (Kelly and Price, 2000). Ligand binding often induces structural changes in proteins, making it one of the most important mechanisms for studying protein conformational dynamics (Bannister and Bannister, 1974). Protein conformation changes at the secondary structure level have been investigated with the help of the far-UV area CD measurements (Rodger et al., 2005; Khrapunov, 2009). CD spectra studies were conducted to assess alpha-helix, beta-sheet, and random coil. The effect of mRA on Aβ protein structural alteration was observed. Changes in the intensity of the spectral peak of proteins reflect secondary structural changes. Initially, the circular dichroism (CD) spectrum of native Aβ$_{1-42}$ was examined to establish its baseline secondary structure. Subsequently, structural changes in Aβ$_{1-42}$ upon binding to mRA were investigated to assess the conformational impact of the interaction. Figure 5A shows the graph of Aβ (1 μM) alone with a clear peak at around 218 nm, which is characteristic of a β-sheet conformation due to aggregation. Therefore, it is evident from this peak that β-sheets are the dominant structure of the Aβ$_{1-42}$ protein. Addition of mRA at varying concentrations (0–10 μM) resulted in an intensity change, indicating binding of mRA to Aβ$_{1-42}$ aggregates and altering the β-sheet structure of the amyloid protein aggregates.

This upward shift in the Aβ protein intensity brought on by the addition of mRA suggests that secondary structural modification is

TABLE 2 Thermodynamics for the interaction of the mRA probe and Aβ protein.

Complex	ΔG (kcal mol^{-1})	ΔH (kcal mol^{-1})	ΔS (cal mol^{-1} K^{-1})	TΔS (cal mol^{-1})
Aβ-mRA	-9.3 ± 0.6	-8.7 ± 0.5	0.8 ± 0.04	229.5 ± 13.6

induced through mRA binding. The structural difference between free $A\beta_{1-42}$ and $A\beta_{1-42}$ bound to mRA is clear from the ellipticity change.

The insertion of mRA significantly affects the $A\beta_{1-42}$ structure. After binding to the mRA, the intensity of $A\beta_{1-42}$ protein changed, indicating a conformational alteration. Without a noticeable change in the shift of the $A\beta_{1-42}$ peak, the change in band intensity indicates that mRA binding causes secondary structural changes. When mRA is added, $A\beta_{1-42}$ ellipticity increases, suggesting the alteration of secondary structure in the protein.

Figure 5B displays the MRE$_{218}$ change (%) of free $A\beta_{1-42}$ and $A\beta_{1-42}$ /mRA complex. Data revealed the influence of mRA on the change in ellipticity at 218 nm of $A\beta_{1-42}$ binding to mRA. These findings showed that in the presence of mRA biosensor, the $A\beta_{1-42}$ protein displayed structural modification. According to these findings, the $A\beta_{1-42}$/mRA complex secondary structure composition changed significantly. Ellipticity values were measured as described elsewhere (Chen et al., 1972; Khan et al., 2002; Rabbani et al., 2014). After mRA treatment at 1,000 nM, the $A\beta_{1-42}$ protein's secondary structure content dropped by 81%. We observed a decrease in the protein's helicity values upon the addition of mRA. These secondary structure changes demonstrate how the amyloid protein undergoes certain structural changes as a result of mRA binding. Given this notable structural change, it's plausible that mRA interacts with Amyloid-Beta via a beta sheet and that this conformational shift serves a detection purpose. Since mRA also changes the structure of the $A\beta_{1-42}$/mRA complex, as observed in the CD spectra, it plays an important role in the helical loss of Aβ structure. Through the formation of hydrogen bonds, the secondary structure may influence both the stiff and flexible structure of proteins (Masuda et al., 2010). These studies revealed that the Aβ protein is β-sheet-rich.

Although the secondary structures of the protein were significantly changed, CD analysis reveals that the majority of Aβ could maintain structural integrity at or below 1,000 nM mRA. Thermodynamic parameters show the changes in free energy and enthalpy, which demonstrate that the complex's structure was altered by differences in the forces interacting between mRA and $A\beta_{1-42}$. The results of thermodynamic and CD experiments are consistent with the fact that Aβ maintained its folded structure despite secondary structural changes. These findings were consistent with the hypothesis that mRA led to complex formation and structural changes in the $A\beta_{1-42}$ protein, which were most likely brought on by the hydrogen bonding.

3.4 Molecular docking of mRA probe binding site on Aβ protein

To understand how the mRA probe and $A\beta_{1-42}$ bind, we conducted a molecular docking study. Investigating molecular interactions that stabilize protein-ligand complexes and locating ligand binding sites in proteins are made possible by molecular docking. Molecular docking simulations revealed that mRA exhibited significant binding affinities with $A\beta_{1-42}$. mRA showed an affinity of -6.5 kcal/mol for $A\beta_{1-42}$ with several close interactions. The docked conformations of mRA were ranked based on their binding affinities, with the top ones analyzed for their interaction profiles and binding stability. These findings suggest that mRA is an effective candidate for targeting $A\beta_{1-42}$ in Alzheimer's disease. Notably, atomic-resolution structures of Aβ fibrils represent rigid, aggregated β-sheet assemblies with limited accessibility to conventional ligand binding pockets. Therefore, to explore the probable binding regions and affinity of mRA, we employed the monomeric Aβ structure, which provides better resolution of individual residue interactions. The docking results with monomeric $A\beta_{1-42}$ should be interpreted as an initial model supporting the molecular recognition process that precedes aggregate formation and binding-induced fluorescence enhancement. Ligand efficiency is another crucial parameter that reflects the potency of a compound relative to its size and was also evaluated for mRA against $A\beta_{1-42}$. The results demonstrated that mRA displayed notable ligand efficiency, underscoring its capability to effectively interact with $A\beta_{1-42}$ with minimal molecular weight. This characteristic strengthens mRA's potential as an appreciable binding partner of $A\beta_{1-42}$.

Detailed analysis of the interactions between mRA and the binding sites of Aβ was performed and depicted in Figure 6. The docked poses of mRA revealed multiple significant interactions with key residues within the binding pockets of the target amyloid protein. These interactions included hydrogen bonds, hydrophobic contacts, and van der Waals forces, crucial for stabilizing the protein-ligand complexes. mRA engaged with several functionally essential residues within the $A\beta_{1-42}$ binding pocket, forming distinct hydrogen bonds and hydrophobic interactions that contributed to its strong binding affinity. $A\beta_{1-42}$ and mRA displayed close contact with critical residues, enhancing their binding stability (Figure 6A). A thorough examination of the docking poses showed that mRA occupied well-defined pockets in $A\beta_{1-42}$, suggesting high specificity and affinity for these targets (Figure 6B). These findings are in good agreement with the fluorescence experiment results.

The binding site interactions were further analyzed and visualized using structural representations. A cartoon representation of Aβ demonstrated the positioning of mRA within its respective binding pockets, which revealed the molecular basis of the interaction. The surface potential views highlighted the regions of $A\beta_{1-42}$ that mRA occupied, reinforcing the stability and compatibility of the docking poses (Figure 6C). The two-dimensional interaction diagrams of mRA probe with $A\beta_{1-42}$ revealed hydrogen bonding and van der Waals interactions as the dominant forces stabilizing the complexes (Figure 6D). Docking studies revealed that probe mRA binds
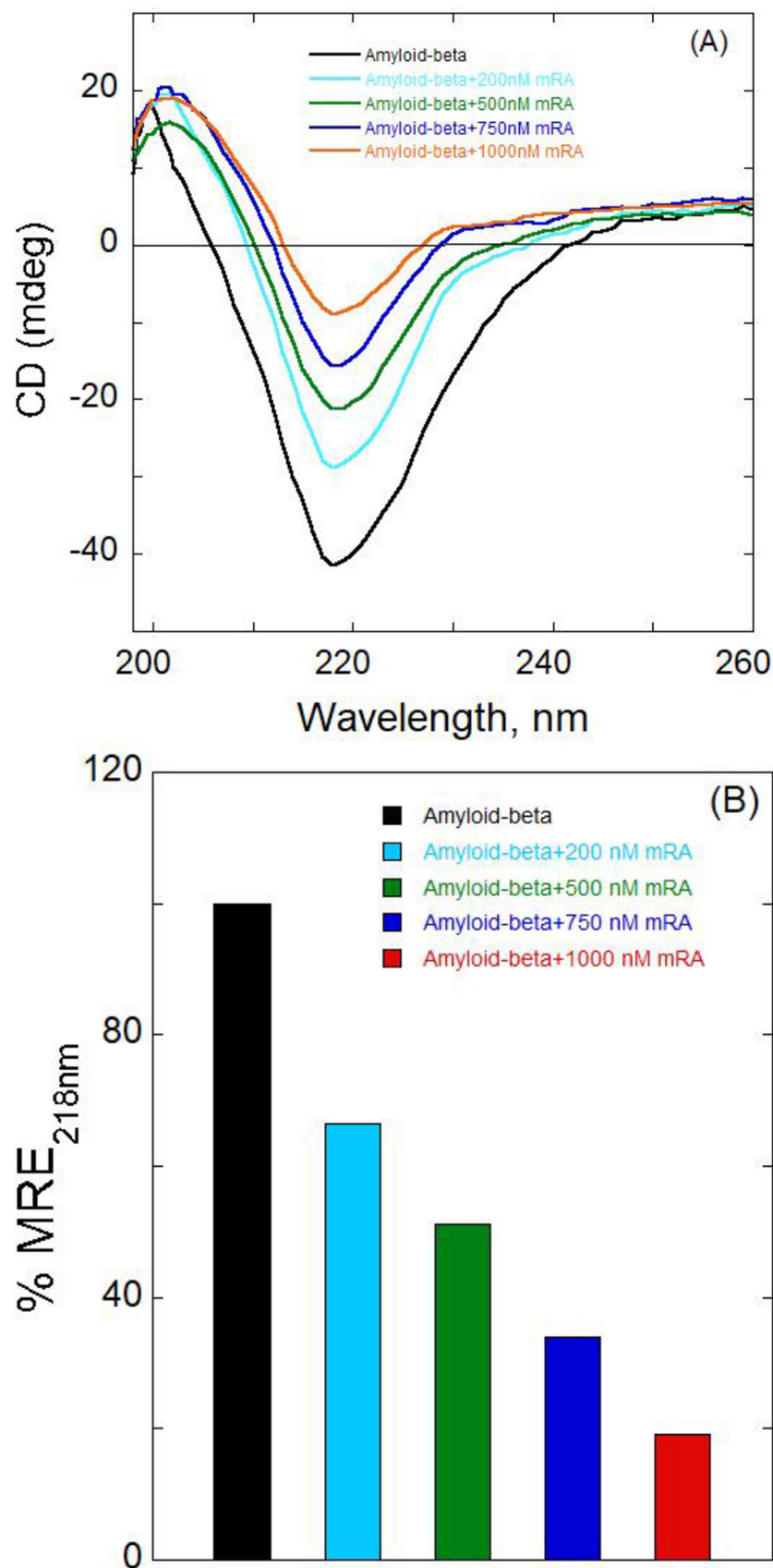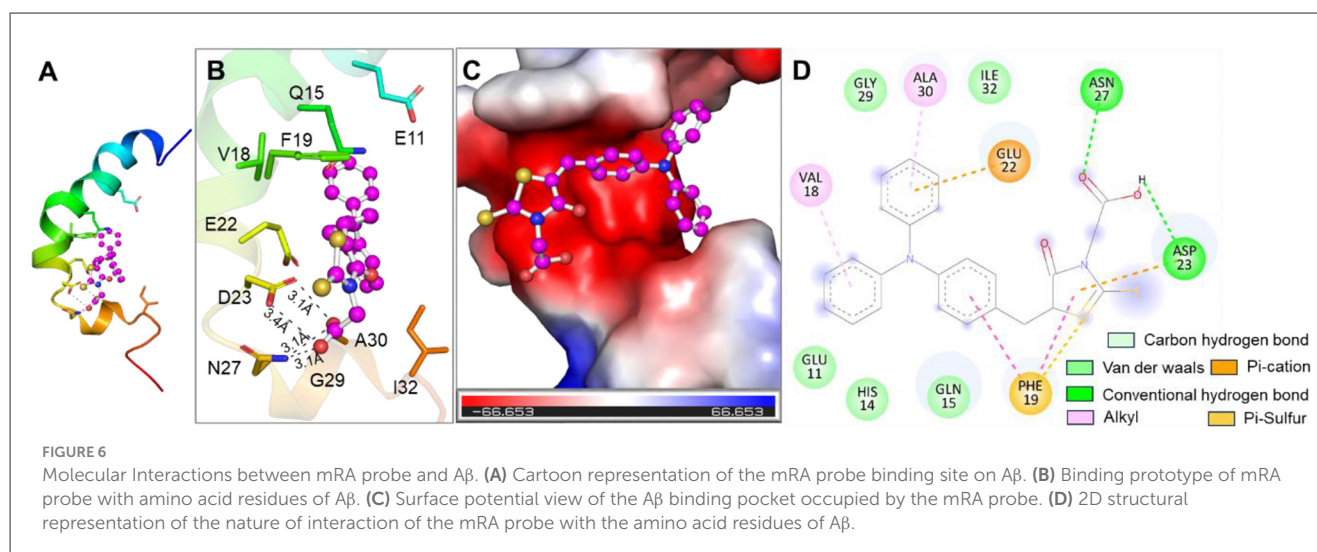
FIGURE 5
Far-UV circular dichroism spectra of Aβ at different Aβ to mRA probe molar ratios. The Aβ protein's ellipticity is considerably altered by adding mRA. (A) The far-UV CD spectra for Aβ (1 μM) in the absence or the presence of different amounts of mRA probe (0−10 μM). **(B)** Displays a bar plot that compares the percent mean residual ellipticity, MRE$_{218nm}$ value of the native protein Aβ, and Aβ in complex with mRA probe.

FIGURE 6
Molecular Interactions between mRA probe and Aβ. **(A)** Cartoon representation of the mRA probe binding site on Aβ. **(B)** Binding prototype of mRA probe with amino acid residues of Aβ. **(C)** Surface potential view of the Aβ binding pocket occupied by the mRA probe. **(D)** 2D structural representation of the nature of interaction of the mRA probe with the amino acid residues of Aβ.

to Aβ through two conventional hydrogen bonds, Asp23 and Asn27, and a carbon-hydrogen bond at Ile32 stabilizes the probe mRA/Aβ complex. Gln15, Glu11, Val18, Phe19, Glu22, His14, Gly29, and Ala30 were also found to be involved in the interaction. mRA has significant binding affinity toward the Aβ at the N/C-terminal region, with a binding free energy of −6.5 kcal/mol for the mRA/Aβ complex formation. These interactions, coupled with favorable binding affinities and ligand efficiency, suggest that probe mRA holds significant potential as an effective binder of Aβ$_{1-42}$. Table 3 lists the summary of fluorophores used for the sensitive detection of amyloid in Alzheimer's disease. To prevent photo-oxidation at 4°C, the mRA probe is kept in the dark and is incredibly stable. This study found good specificity and sensitivity in the quick detection of amyloid in bodily fluids, although various fluorescent probes have been reported.

3.5 Specificity and cross-activity

The specific recognition of the Aβ protein in complex biological fluids by the molecular probe is a crucial factor for accurately detecting the target. As a consequence, we observed the fluorescence intensity of mRA treated with several other interfering molecular species, such as trypsin, GDF-15, collagen, gelatin, DNase, RNase, chitosan, bovine serum albumin (BSA), and human serum albumin (HSA), under the same conditions. As illustrated in Figure 7, HSA and BSA exhibited a significant increase in the fluorescence emission. Most of the biomolecules showed an insignificant influence on the fluorescence enhancement, except Aβ, as well as BSA and HSA. The mechanism of mRA fluorescence enhancement in HSA is due to the site-specific binding of mRA in binding site IIIA of the HSA protein. The mRA interaction sites in the binding site lock the intermolecular mobility of mRA, which triggers the fluorescence emission in the mRA/HSA complex (Chinnappan et al., 2025). The influence of the fluorescence signal by BSA is due to its sequence similarity with HSA, which would
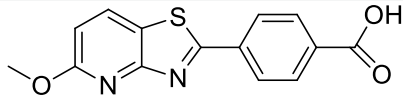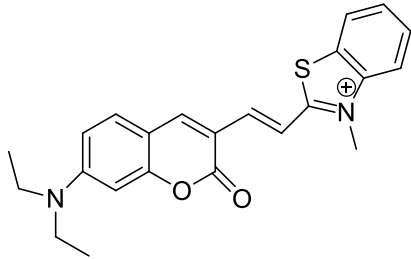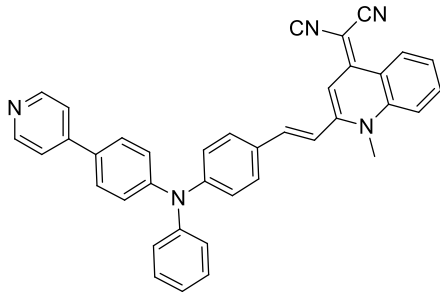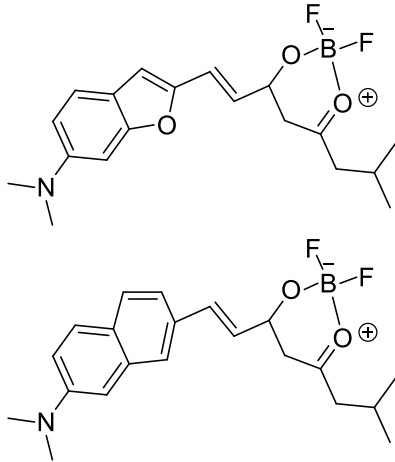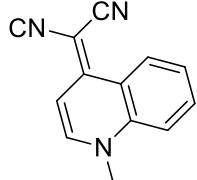
bind mRA in the same way. These results indicate that mRA is a potential fluorescent probe for the sensitive and specific detection of Aβ$_{1-42}$ protein from biological fluids.

4 Conclusions

This study systematically characterized the interaction mechanism responsible for the mRA biosensor with Aβ$_{1-42}$. mRA is proposed as a recognition molecule that shows outstanding advantages in Aβ binding and early detection. Binding of mRA to Aβ$_{1-42}$ was investigated by the fluorescence spectroscopy results, which revealed strong interaction ($K_a = 3.0 \times 10^{-6}$ M^{-1}) at 298 K. A change in fluorescence and a significant reduction in affinity on increasing temperature showed that mRA/Aβ complex formation results in static fluorescence enhancement. Additionally, we obtained a negative ΔG value from the Van't Hoff equation, which indicated that the reaction was spontaneous and thermodynamically beneficial. Data from the thermodynamics of mRA with Aβ showed that hydrogen bonds and van der Waals interactions are the main ways that mRA and Aβ$_{1-42}$ protein interact. Aβ far-UV CD spectra went upward in the presence of mRA, suggesting the formation of the Aβ$_{1-42}$/mRA complex. The results of thermostability and fluorescence binding demonstrate that mRA attaches to Aβ$_{1-42}$ with a high binding energy and uses a variety of bonding forces to make several tight contacts with crucial residues.

In summary, this study demonstrates the binding mechanism of mRA to Aβ$_{1-42}$. This is the first study to look at the mechanism of interaction between the therapeutically relevant mRA and the Aβ$_{1-42}$ protein, which is important in AD. Understanding the mechanism of interaction between mRA and Aβ$_{1-42}$ will aid in comprehending the forces that lead to this connection, and the particulars of these forces result in the construction of a stable complex. This study provides insight into the binding mechanism of mRA with Aβ$_{1-42}$ and can be very helpful for the early detection and progression of amyloid accumulation in

TABLE 3 Summary of various types of fluorophores used for the sensitive detection of Aβ.

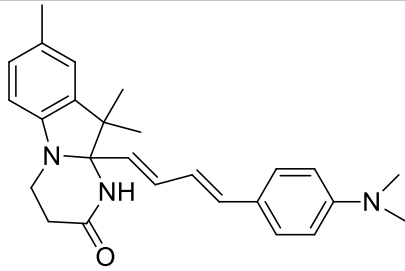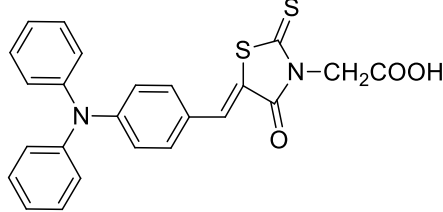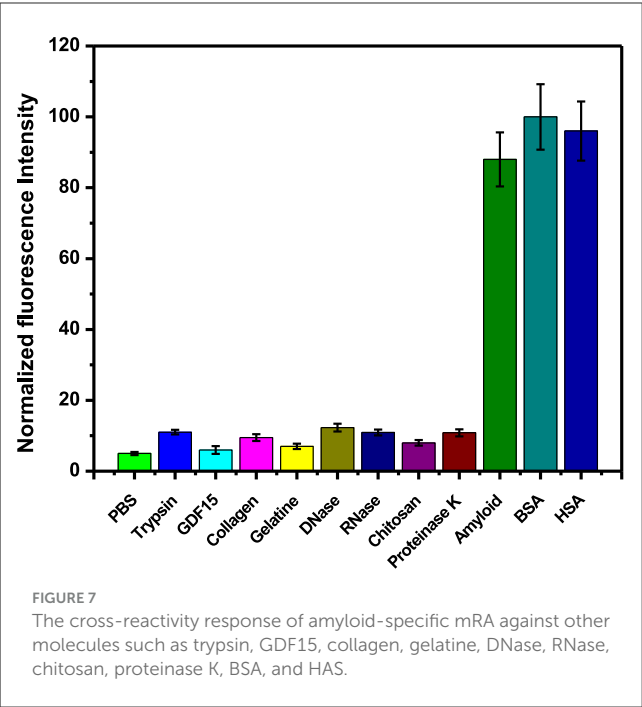| Probe Name	Structure	Method used	Fold enhancement	Ref
Pyridothiazole derivative		Cu(II) induced turn-on fluorescence	1μM	(Gour et al., 2018)
Hemicyanine-based benzothiazole-coumarin		Aβ$_{42}$ aggregates through switch-on, enhanced fluorescence	30	(Rajasekhar et al., 2016)
PTPA-QM		Aggregation-induced emission fluorescent probe,	22	(Fang et al., 2023)
N,N-dimethyl biannulated electron-donating groups: BZ-OB (benzofuran) and NAP-OB (naphthalene)		Polarity induced fluorescence/Fluorescence Imaging	20.5(BZ-OB) 69.4 (NAP-OB)	(An et al., 2022)
quinoline-based AIE probe(FB)		Aggregation-induced emission	20	(Wang et al., 2020)

(Continued)

TABLE 3 (Continued)

Probe Name	Structure	Method used	Fold enhancement	Ref
2,1,3-benzothiadiazole (BTD)		Two-photon fluorescence imaging	6	(Chen et al., 2024)
NPBZ		*in vivo* imaging	47	(Lv et al., 2025)
BPM1		Aβ Aggregation-induced emission	10	(Zhao et al., 2023)
LDS722		Fluorescence turn-on emission	200	(Warerkar et al., 2021)
1,7-bis[(2,5-dimethoxy-3-diethylamino)phenyl]-1,6-heptadiene−3,5-dione (curcumin-based NIR Dye)		Fluorescence turn-on emission	19.5	(Si et al., 2019)
Thioflavin X		Aβ Aggregation-induced emission/ Fluorescence Imaging	7	(Needham et al., 2020)
Diethyl 6-(dimethylamino) naphthalene2,3-dicarboxylate (DMNDC)		Aβ Aggregation-induced intramolecular charge transfer (ICT) emission	10	(Das et al., 2020)
(2-((1E,3E)-4-(4-(dimethylamino)phenyl)buta-1,3-dien-1-yl)-1,1,3-trimethyl-1H-benzo[e]indol-3-ium iodide)		Aβ Aggregation-induced emission/ Fluorescence Imaging	–	(Lee et al., 2019)

(Continued)

TABLE 3 (Continued)

Probe Name	Structure	Method used	Fold enhancement	Ref
THK-565		Fluorescence Imaging	16	(Naganuma et al., 2023)
Triphenylamine rhodamine-3-acetic (mRA)		Fluorescence turn-on emission	24	This work

FIGURE 7
The cross-reactivity response of amyloid-specific mRA against other molecules such as trypsin, GDF15, collagen, gelatine, DNase, RNase, chitosan, proteinase K, BSA, and HAS.

AD. Their biological significance and applications in targeting the $A\beta_{1-42}$ to detect progression and accumulation in AD may become clearer with more research into the unique structural traits and functional consequences of mRA in clinical samples with cells of amyloid translation beginning. These findings have strengthened our confidence in the early diagnosis and treatment of AD in the analysis of $A\beta_{1-42}$ aggregates, the development of new identification probes, and the quantification of $A\beta_{1-42}$. This is a preliminary study of a specific fluorescent probe against Aβ. More detailed research is necessary to understand mRA and $A\beta_{1-42}$ interactions for implementing mRA in AD-related clinical applications.

Data availability statement

The original contributions presented in the study are included in the article/Supplementary material, further inquiries can be directed to the corresponding author/s.

Author contributions

RC: Funding acquisition, Writing – original draft, Writing – review & editing, Formal analysis, Data curation, Conceptualization, Validation. MK: Conceptualization, Funding acquisition, Validation, Writing – review & editing, Formal analysis, Writing – original draft, Methodology. TM: Software, Writing – review & editing, Formal analysis, Data curation. SA: Formal analysis, Writing – review & editing. SE: Writing – review & editing, Formal analysis, Methodology. AY: Supervision, Methodology, Writing – review & editing, Resources. SD: Data curation, Writing – review & editing. TM: Formal analysis, Writing – review & editing. IH: Software, Writing – review & editing, Formal analysis.

Funding

Conflict of interest

The authors declare that the research was conducted in the absence of any commercial or financial relationships that could be construed as a potential conflict of interest.

The author(s) declared that they were an editorial board member of Frontiers, at the time of submission. This had no impact on the peer review process and the final decision.

Generative AI statement

The author(s) declare that no Gen AI was used in the creation of this manuscript.

Publisher's note

All claims expressed in this article are solely those of the authors and do not necessarily represent those of their affiliated organizations, or those of the publisher, the editors and the reviewers. Any product that may be evaluated in this article, or claim that may be made by its manufacturer, is not guaranteed or endorsed by the publisher.

Supplementary material

The Supplementary Material for this article can be found online at: https://www.frontiersin.org/articles/10.3389/fnins.2025.1653063/full#supplementary-material

References

An, J., Verwilst, P., Aziz, H., Shin, J., Lim, S., Kim, I., et al. (2022). Picomolar-sensitive β-amyloid fibril fluorophores by tailoring the hydrophobicity of biannulated π-elongated dioxaborine-dyes. *Bioact. Mater.* 13, 239–248. doi: 10.1016/j.bioactmat.2021.10.047

Avila, J., Lucas, J. J., Perez, M., and Hernandez, F. (2004). Role of tau protein in both physiological and pathological conditions. *Physiol. Rev.* 84, 361–384. doi: 10.1152/physrev.00024.2003

Bank, P. D. (1971). Protein data bank. *Nat. New Biol* 233, 10–1038.

Bannister, W., and Bannister, J. (1974). Evidence for the validity of three-component fitting of protein circular dichroism spectra. *Z. Für Naturforschung C* 29, 9–11. doi: 10.1515/znc-1974-1-204

Barghorn, S., Nimmrich, V., Striebinger, A., Krantz, C., Keller, P., Janson, B., et al. (2005). Globular amyloid β-peptide1– 42 oligomer– a homogenous and stable neuropathological protein in Alzheimer's disease. *J. Neurochem.* 95, 834–847. doi: 10.1111/j.1471-4159.2005.03407.x

Bradford, M. M. (1976). A rapid and sensitive method for the quantitation of microgram quantities of protein utilizing the principle of protein-dye binding. *Anal. Biochem.* 72, 248–254. doi: 10.1016/0003-2697(76)90527-3

Chen, M., Zhang, Z., Shi, Z., Sun, J., and Gao, F. (2024). A facile two-photon red-emission fluorescent marker with a large stokes shift for *in vivo* brain imaging of amyloid-beta aggregates. *Cell Rep. Phys. Sci.* 5:101810. doi: 10.1016/j.xcrp.2024.101810

Chen, Y-. H., Yang, J. T., and Martinez, H. M. (1972). Determination of the secondary structures of proteins by circular dichroism and optical rotatory dispersion. *Biochemistry* 11, 4120–4131. doi: 10.1021/bi00772a015

Chinnappan, R., Mir, T. A., Easwaramoorthi, S., Sunil, G., Feba, A., Kanagasabai, B., et al. (2025). Molecular engineering of a fluorescent probe for highly efficient detection of human serum albumin in biological fluid. *Sens. Int.* 6, 100304. doi: 10.1016/j.sintl.2024.100304

Das, A., Dutta, T., Gadhe, L., Koner, A. L., Saraogi, I. (2020). Biocompatible fluorescent probe for selective detection of amyloid fibrils. *Anal. Chem.* 92, 10336–10341. doi: 10.1021/acs.analchem.0c00379

DeLano, W. L. (2002). Pymol: an open-source molecular graphics tool. *CCP4 Newsl Protein Crystallogr.* 40, 82–92. Available online at: https://legacy.ccp4.ac.uk/newsletters/newsletter40/11_pymol.pdf

Fang, Y., Wang, Q., Xiang, C., Liu, G., and Li, J. (2023). A novel aggregation-induced emission fluorescent probe for detection of β-amyloid based on pyridinyltriphenylamine and Quinoline–Malononitrile. *Biosensors* 13:610. doi: 10.3390/bios13060610

Gour, N., Kshtriya, V. S., Koshti, B., Gupta, S., and Patel, D. (2018). A new fluorescence probe for rapid detection of amyloid. *Chemrxiv.* doi: 10.26434/chemrxiv.6982895.v1

Hampel, H., Hardy, J., Blennow, K., Chen, C., Perry, G., Kim, S. H., et al. (2021). The amyloid-β pathway in Alzheimer's disease. *Mol. Psychiat.* 26, 5481–5503. doi: 10.1038/s41380-021-01249-0

Howie, A. J., and Brewer, D. B. (2009). Optical properties of amyloid stained by Congo red: history and mechanisms. *Micron* 40, 285–301. doi: 10.1016/j.micron.2008.10.002

Kayed, R., Pensalfini, A., Margol, L., Sokolov, Y., Sarsoza, F., Head, E., et al. (2009). Annular protofibrils are a structurally and functionally distinct type of amyloid oligomer. *J. Biol. Chem.* 284, 4230–4237. doi: 10.1074/jbc.M808591200

Kelly, S. M., and Price, N. C. (2000). The use of circular dichroism in the investigation of protein structure and function. *Curr. Protein Pept. Sci.* 1, 349–384. doi: 10.2174/1389203003381315

Khan, M. A. (2022). Ferritin iron responsive elements (IREs) mRNA interacts with eIF4G and activates *in vitro* translation. *Front. Biosci.-Elite* 14:17. doi: 10.31083/j.fbe1403017

Khan, M. A., Kumar, Y., and Tayyab, S. (2002). Bilirubin binding properties of pigeon serum albumin and its comparison with human serum albumin. *Int. J. Biol. Macromol.* 30, 171–178. doi: 10.1016/S0141-8130(02)00017-X

Khan, M. A., Mohammad, T., Malik, A., Hassan, M. I., and Domashevskiy, A. V. (2023). Iron response elements (IREs)-mRNA of Alzheimer's amyloid precursor protein binding to iron regulatory protein (IRP1): a combined molecular docking and spectroscopic approach. *Sci. Rep.* 13:5073. doi: 10.1038/s41598-023-32073-x

Khan, M. A., Walden, W. E., Theil, E. C., and Goss, D. J. (2017). Thermodynamic and kinetic analyses of iron response element (IRE)-mRNA binding to iron regulatory protein, IRP1. *Sci. Rep.* 7:8532. doi: 10.1038/s41598-017-09093-5

Khrapunov, S. (2009). Circular dichroism spectroscopy has intrinsic limitations for protein secondary structure analysis. *Anal. Biochem.* 389, 174–176. doi: 10.1016/j.ab.2009.03.036

Kubota, R., and Hamachi, I. (2015). Protein recognition using synthetic small-molecular binders toward optical protein sensing *in vitro* and in live cells. *Chem. Soc. Rev.* 44, 4454–4471. doi: 10.1039/C4CS00381K

Lee, M., Kim, M., Tikum, A. F., Lee, H. J., Thamilarasan, V., Lim, M. H., et al. (2019). A near-infrared fluorescent probe for amyloid-β aggregates. *Dyes Pigm.* 162, 97–103. doi: 10.1016/j.dyepig.2018.10.013

Lv, J., Li, H., Gao, J., Dong, N., Shi, W., Ma, H., et al. (2025). A dual-functional fluorescence probe for simultaneous *in vivo* imaging of Aβ aggregates and hydrogen peroxide in the brain of mice with Alzheimer's disease. *CCS Chem.* 1–22. doi: 10.31635/ccschem.025.202404927

Mallesh, R., Khan, J., Gharai, P. K., Ghosh, S., Garg, S., Arshi, M. U., et al. (2023). High-affinity fluorescent probes for the detection of soluble and insoluble Aβ deposits in Alzheimer's disease. *ACS Chem. Neurosci.* 14, 1459–1473. doi: 10.1021/acschemneuro.2c00787

Mallesh, R., Khan, J., Pradhan, K., Roy, R., Jana, N. R., Jaisankar, P., et al. (2022). Design and development of benzothiazole-based fluorescent probes for selective detection of Aβ aggregates in Alzheimer's disease. *ACS Chem. Neurosci.* 13, 2503–2516. doi: 10.1021/acschemneuro.2c00361

Masuda, T., Goto, F., Yoshihara, T., and Mikami, B. (2010). The universal mechanism for iron translocation to the ferroxidase site in ferritin, which is mediated by the well conserved transit site. *Biochem. Biophys. Res. Commun.* 400, 94–99. doi: 10.1016/j.bbrc.2010.08.017

Mohammad, T., Mathur, Y., and Hassan, M. I. (2021). InstaDock: a single-click graphical user interface for molecular docking-based virtual high-throughput screening. *Brief. Bioinform.* 22:bbaa279. doi: 10.1093/bib/bbaa279

Naganuma, F., Murata, D., Inoue, M., Maehori, Y., Harada, R., Furumoto, S., et al. (2023). A novel near-infrared fluorescence probe THK-565 enables *in vivo* detection of amyloid deposits in Alzheimer's disease mouse model. *Mol. Imaging Biol.* 25, 1115–1124. doi: 10.1007/s11307-023-01843-4

Nasica-Labouze, J., Nguyen, P. H., Sterpone, F., Berthoumieu, O., Buchete, N-. V., Coté, S., et al. (2015). Amyloid β protein and Alzheimer's disease: when computer simulations complement experimental studies. *Chem. Rev.* 115, 3518–3563. doi: 10.1021/cr500638n

Needham, L.-M., Weber, J., Varela, J. A., Fyfe, J. W. B., Do, D. T., Xu, C. K., et al. (2020). ThX - a next-generation probe for the early detection of amyloid aggregates. *Chem. Sci.* 11, 4578–4583. doi: 10.1039/C9SC04730A

Novo, M., Freire, S., and Al-Soufi, W. (2018). Critical aggregation concentration for the formation of early Amyloid-β (1–42) oligomers. *Sci. Rep.* 8:1783. doi: 10.1038/s41598-018-19961-3

Puchtler, H., Sweat, F., and Levine, M. (1959). Fluorescent stains, with special reference to amyloid and connective tissues. *Arch. Pathol.* 68, 487–498.

Qin, J., Cho, M., and Lee, Y. (2019). Ultrasensitive detection of amyloid-β using cellular prion protein on the highly conductive Au nanoparticles–poly(3,4-ethylene dioxythiophene)–poly(thiophene-3-acetic acid) composite electrode. *Anal. Chem.* 91, 11259–11265. doi: 10.1021/acs.analchem.9b02266

Qin, J., Jo, D. G., Cho, M., and Lee, Y. (2018). Monitoring of early diagnosis of Alzheimer's disease using the cellular prion protein and poly(pyrrole-2-carboxylic acid) modified electrode. *Biosens. Bioelectron.* 113, 82–87. doi: 10.1016/j.bios.2018.04.061

Rabbani, G., Kaur, J., Ahmad, E., Khan, R. H., and Jain, S. K. (2014). Structural characteristics of thermostable immunogenic outer membrane protein from Salmonella enterica serovar Typhi. *Appl. Microbiol. Biotechnol.* 98, 2533–2543. doi: 10.1007/s00253-013-5123-3

Rajasekhar, K., Narayanaswamy, N., Murugan, N. A., Kuang, G., Agren, H., and Govindaraju, T. (2016). A high affinity red fluorescence and colorimetric probe for amyloid β aggregates. *Sci. Rep.* 6:23668. doi: 10.1038/srep23668

Ren, H-. X., Miao, Y-. B., and Zhang, Y. (2020). An aptamer-based fluorometric assay for amyloid-β oligomers using a metal-organic framework of type Ru@MIL-101(Al) and enzyme-assisted recycling. *Microchim. Acta* 187:114. doi: 10.1007/s00604-019-4092-3

Rodger, A., Marrington, R., Roper, D., and Windsor, S. (2005). "Circular Dichroism Spectroscopy for the Study of Protein-Ligand Interactions," in *Protein-Ligand Interactions: Methods and Applications*, ed. G. Ulrich Nienhaus (Totowa, NJ: Humana Press), 343–363. doi: 10.1385/1-59259-912-5:343

Ross, P. D., and Subramanian, S. (1981). Thermodynamics of protein association reactions: forces contributing to stability. *Biochemistry* 20, 3096–3102. doi: 10.1021/bi00514a017

Scheltens, P., Blennow, K., Breteler, M. M., de Strooper, B., Frisoni, G. B., Salloway, S., et al. (2016). Alzheimer's disease. *Lancet.* 388, 505–517. doi: 10.1016/S0140-6736(15)01124-1

Selkoe, D. J. (2001). Alzheimer's disease: genes, proteins, and therapy. *Physiol. Rev.* 81, 741–766. doi: 10.1152/physrev.2001.81.2.741

Sharma, P. K., Kim, E-. S., Mishra, S., Ganbold, E., Seong, R-. S., Kim, Y. M., et al. (2022). Ultrasensitive probeless capacitive biosensor for amyloid beta (Aβ1-42) detection in human plasma using interdigitated electrodes. *Biosens. Bioelectron.* 212:114365. doi: 10.1016/j.bios.2022.114365

Si, G., Zhou, S., Xu, G., Wang, J., Wu, B., and Zhou, S. (2019). A curcumin-based NIR fluorescence probe for detection of amyloid-beta (Aβ) plaques in Alzheimer's disease. *Dyes Pigm.* 163, 509–515. doi: 10.1016/j.dyepig.2018.12.003

Tayyab, S., Sam, S. E., Kabir, Md. Z., Ridzwan, N. F. W., and Mohamad, S. B. (2019). Molecular interaction study of an anticancer drug, ponatinib with human serum albumin using spectroscopic and molecular docking methods. *Spectrochim. Acta. A. Mol. Biomol. Spectrosc.* 214, 199–206. doi: 10.1016/j.saa.2019.02.028

Thamaraiselvi, P., Duraipandy, N., Kiran, M. S., and Easwaramoorthi, S. (2019). Triarylamine rhodanine derivatives as red emissive sensor for discriminative detection of Ag+ and Hg2+ ions in buffer-free aqueous solutions. *ACS Sustain. Chem. Eng.* 7, 9865–9874. doi: 10.1021/acssuschemeng.9b00417

Trusova, V., Tarabara, U., Zhytniakivska, O., Vus, K., and Gorbenko, G. (2022). Förster resonance energy transfer analysis of amyloid state of proteins. *BBA Adv.* 2:100059. doi: 10.1016/j.bbadva.2022.100059

Visualizer, D. (2005). *Discovery Studio Visualizer (version 2.0)*. San Diego, CA: Accelrys software inc.

Wang, Y., Qiu, Y., Sun, A., Xiong, Y., Tan, H., Shi, Y., et al. (2020). Dual-functional AIE fluorescent probes for imaging β-amyloid plaques and lipid droplets. *Anal. Chim. Acta* 1133, 109–118. doi: 10.1016/j.aca.2020.07.073

Warerkar, O. D., Mudliar, N. H., and Singh, P. K. (2021). A hemicyanine based fluorescence turn-on sensor for amyloid fibril detection in the far-red region. *J. Mol. Liq.* 328:115322. doi: 10.1016/j.molliq.2021.115322

Zhang, Y., Ding, C., Li, C., and Wang, X. (2021). "Chapter Four - Advances in fluorescent probes for detection and imaging of amyloid-β peptides in Alzheimer's disease," in *Advances in Clinical Chemistry*, ed. G. S. Makowski (Amsterdam: Elsevier), 135–190.

Zhao, M., Zhang, G., Huang, S., Zhang, J., Zhu, Y., Zhu, X., et al. (2023). An activatable small-molecule fluorogenic probe for detection and quantification of beta-amyloid aggregates. *Spectrochim. Acta. A. Mol. Biomol. Spectrosc.* 303:123145. doi: 10.1016/j.saa.2023.123145